Comparison of CIS- and EOM-CCSD-Calculated Adiabatic Excited-State Structures. Changes in Charge Density on Going to Adiabatic Excited States

Kenneth B. Wiberg,*,† Yi-gui Wang,† Anselmo E. de Oliveira,†,‡ S. Ajith Perera,§ and Patrick H. Vaccaro*,†

Department of Chemistry, Yale University, New Haven, Connecticut 06520-8107, and The Quantum Theory Project, University of Florida, Gainsville, Florida 32611

Received: August 17, 2004

The CIS and EOM-CCSD adiabatic geometries for the first excited states of a set of small molecules (C_2H_4, C_2H_2, $H_2C{=}O$, $H_2C{=}S$, CS_2, CO_2, SO_2, NO_2) have been calculated using the 6-311++G** basis set to see if the former geometries can be good starting points for optimizations at the latter theoretical level. With most of the molecules, there is fairly good agreement between the results from the two methods, and EOM-CCSD gives good agreement with the available experimental data. A detailed discussion of the lowest-lying singlet excited states in CO_2 and CS_2 is presented, highlighting the pronounced differences in electronic character and equilibrium structure displayed by these isovalent species. The origins of the structural distortions that are frequently found for the adiabatic excited states are examined with the aid of deformation density plots and the electron localization function (ELF).

1. Introduction

Electronically excited states frequently have significantly different structures than ground states. For example, the $\pi^* \leftarrow n$ state of formaldehyde is known to have a pyramidal structure,[1] and the $\pi^* \leftarrow \pi$ state of acetylene has a bent structure.[2] CIS[3] and EOM-CCSD[4] represent two extremes in single-reference models for calculating the structures and energies of electronically excited states. CIS is computationally inexpensive and allows facile geometry optimizations for excited states in addition to giving vibrational frequencies. However, it often leads to significant errors in the calculated transition energies.[5] EOM-CCSD is very effective in reproducing experimental transition energies,[6] but it is also computationally intensive, making it relatively difficult to use to obtain the structures of excited states.

We have examined the question of whether the CIS-optimized structures for the adiabatic excited states would provide good starting points for EOM-CCSD geometry optimizations for these states. The calculations were carried out using the 6-311++G** basis set, which has been found to give good transition energies for CCSD-EOM calculations of valence states and the lower-energy Rydberg states.[7] It might be noted that this basis set gives lower total energies and generally more satisfactory ground-state geometries than aug-cc-pVDZ,[8] and it also gives lower energies for excited states. The higher-energy Rydberg states require the addition of more diffuse functions to obtain satisfactory calculated transition energies.[7] However, these states are not of concern in this report.

2. Ethylene

Ethylene is one of the most studied of organic compounds. The equilibrium C=C bond length has been derived from experimental data,[9] and many calculations have been reported.[10] The electronically excited states have received extensive study, both experimentally[11] and theoretically.[11]

The lowest-energy transition is to a 3s $\leftarrow \pi$ Rydberg state, and this is followed by the $\pi^* \leftarrow \pi$ excited state. The latter is known to be twisted[12] to minimize the interaction between the singly occupied π and π^* orbitals. The former has also been found to be twisted, but to a smaller degree than the $\pi^* \leftarrow \pi$ excited state. Experimental information concerning the geometries of these excited states is available,[12] and they are compared with the results of CIS and EOM-CCSD calculations in Table 1.

The HF level for the ground state corresponds to the CIS level for the excited states. The HF carbon−carbon double bond is short as is normally found for multiple bonds at this level of theory.[13] The CCSD-calculated length is in very good agreement with the observed value.

The adiabatic $\pi^* \leftarrow \pi$ excited state is known to be twisted, and both CIS and CCSD give structures twisted by ~90°. The C=C bond length was found to be somewhat increased in the excited state. EOM-CCSD gives a slightly enlarged bond, whereas CIS gives a considerably elongated bond. The planar transition state for rotation about the C=C bond is calculated to have an energy about 14 000 cm^{-1} higher than the adiabatic state and to be considerably elongated.

The adiabatic 3s $\leftarrow \pi$ Rydberg state is known to have a C=C bond length of 1.41 Å, and this is reproduced by both CIS and EOM-CCSD. The EOM-CCSD potential energy curve for twisting the C=C bond has a very shallow minimum at 27° (Figure S1, Supporting Information), in good agreement with the experimental results. The CIS calculation gives only a planar structure for this state.

3. Acetylene

An analysis of the structure of the $\tilde{A}^1A_u$ $\pi^* \leftarrow \pi$ transition for acetylene has shown that it adopts a trans-bent geometry.[2]

* To whom correspondence should be addressed. E-mail: kenneth.wiberg@yale.edu (K.W.).
† Yale University
‡ Present address: Instituto de Quimica-UFG, Goiania, GO, Brazil.
§ University of Florida.

10.1021/jp040558j CCC: $30.25
Published on Web 12/31/2004

TABLE 1: Results of CIS and EOM-CCSD Calculations for Ethylene

state	level	r(C−C) (Å)	r(C−H) (Å)	∠HCC (deg)	∠HCCH (deg)	TE[a] (eV)	barrier[b] (cm^{-1})
$\tilde{X}^1A_g$ (GS)	expt[9]	1.339	1.087	121.7	0.0		
	CCSD	1.337	1.086	121.5	0.0		
	HF	1.319	1.076	121.6	0.0		
$\tilde{A}^1B_{1u}$	expt[12]	1.4			37−90	5.5	
($^1B_1$, $\pi^* \leftarrow \pi$)	EOM-CCSD	1.344	1.090	123.9	87.0[c]	5.98	14200
	CIS	1.373	1.091	123.5	88.5[c]	5.61	13200
$\tilde{A}^1B_{1u}$ (TS)	EOM-CCSD	1.480	1.085	120.4	0.0	7.75	
	CIS	1.496	1.074	120.0	0.0	7.25	
$\tilde{B}^1B_{3u}$	expt[12]	1.41	1.08	117.8	37.0	7.11	
($^1B_3$, $3s \leftarrow \pi$)	EOM-CCSD	1.388	1.089	119.9	27.0	7.19	97
	CIS	1.418	1.074	119.7	0.0	7.01	*d*
$\tilde{B}^1B_{3u}$ (TS)	EOM-CCSD	1.412	1.093	119.8	0.0	7.20	
	CIS	*d*					

[a] Transition energy. [b] Barrier to rotation to a planar structure. [c] Single-reference method not appropriate for the 90°-rotated structure. [d] Optimization using CIS led to a planar structure.

TABLE 2: Results of CIS and CCSD-EOM Calculations for Acetylene

state	level	r(CC) (Å)	r(CH) (Å)	∠H−C−C (deg)	TE[a] (eV)	barrier[b] (cm^{-1})
$\tilde{X}^1\Sigma_g^+$ (GS)	expt[15]	1.208	1.057	180		
	CCSD (full)	1.209	1.066	180		
	SCF	1.183	1.056	180		
$\tilde{A}^1A_u$	expt [2]	1.375	1.097	122.5	5.23	
	EOM-CCSD	1.364	1.099	123.6	5.53	10412
	CIS	1.356	1.082	124.6	4.59	9676
$\tilde{A}^1A_u$	EOM-CCSD	1.322	1.066	180	6.82	
($^1\Sigma_u^-$, TS)	CIS	1.318	1.054	180	5.79	

[a] Transition energy. [b] Barrier to linear TS.

This has been confirmed by a number of theoretical studies.[14] The results of our calculations for the ground state and the excited state using both CIS and EOM-CCSD are given in Table 2. The ground-state CCSD structure is quite satisfactory,[15] and the SCF geometry is fairly good, with a somewhat shorter (0.02 Å) triple bond.

The excited-state EOM-CCSD-calculated structure is again in good agreement with the experimental structure. The CIS structure is also satisfactory and reproduces the C≡C−H bond angle quite well. Thus, the CIS structure would again be a good starting point for a higher-level geometry optimization.

The change in geometry on going from the ground state to the $\pi-\pi^*$ excited state probably has an origin similar to that for ethylene. It is, of course, not possible for the molecule to rotate to minimize the interaction between the singly occupied orbitals derived from one set of π and π^*. However, localizing the π^* orbital serves the same purpose. Thus, the carbons should go from being linear in the ground state to trigonal in the excited state.

This expectation can be confirmed by examining the deformation density plots that give the difference in charge density between the molecule and a set of spherically symmetrical atoms at the nuclear positions of the molecule (see below) (Figure 1). In the ground state, there is an increase in charge density in the C−H bonding regions and at the center of the C≡C bond. The bent excited state has regions of nonbonded charge density that correspond to the expected changes. Additional information concerning the ground and excited states (AIM analysis[16] and ELF analysis[17]) can be found in the Supporting Information.

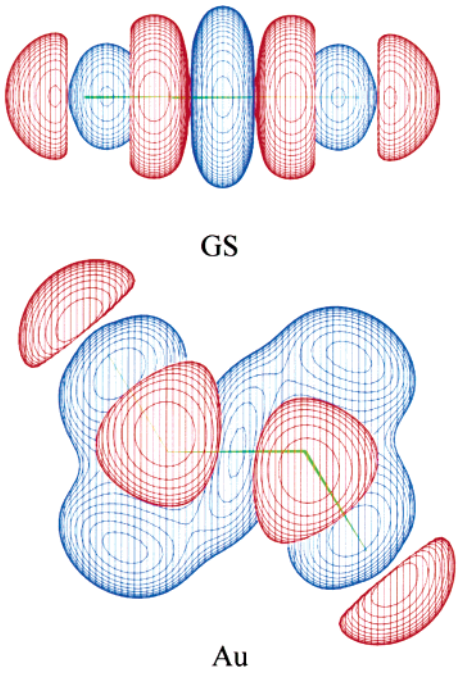

Figure 1. Deformation density plots for the ground state and excited state of acetylene. The excited state has regions of charge density opposite to the hydrogens, leading to effectively trigonal bonding for the carbons.

4. Formaldehyde

The ground[18] and excited states of formaldehyde have received extensive study both experimentally[1,19] and theoretically.[20] An examination of the rovibrational structure of the $\pi^* \leftarrow n_y$ (A″) electronic transition has shown that the relaxed geometry is pyramidal with an out-of-plane bending angle of about 34°.[1,18] The CIS and EOM-CCSD-calculated structures are compared with the experimental results in Table 3. The HF- and CCSD-optimized structures for the ground state are included in the table. The ground-state geometry is well reproduced by the CCSD model, and the SCF geometry has a short C═O bond, as is generally found.[13]

The EOM-CCSD $\pi^* \leftarrow n_y$ relaxed excited-state structure is in good accord with the experimental structure. If the CIS result is corrected for the short C═O ground-state bond length, it is in reasonable agreement with the experimental structure and would provide a good starting point for the higher-level geometry optimization.

The EOM-CCSD calculation predicts an adiabatic transition energy of 3.7 eV, in good accord with the experimental value (3.5 eV). The CIS result, 4.5 eV, is much less satisfactory. Another useful comparison of the two methods is the barrier to inversion for the pyramidal structure. The calculated value is

TABLE 3: Calculated and Observed Relaxed Structures for Formaldehyde Excited States

state	level	r(C=O) (Å)	r(C−H) (Å)	∠HCH (deg)	α[a]	TE[b] (eV)	barrier[c] (cm^{-1})
$\tilde{X}^1A_1$ (GS)	expt[18]	1.203	1.101	116.3	0.0		
	CCSD (full)	1.206	1.106	116.1	0.0		
	HF	1.180	1.094	116.2	0.0		
$\tilde{A}^1A_2$	expt[1,19]	1.323	1.103	118.1	34	3.495	316
($^1A''$, $\pi^* \leftarrow n_y$)	EOM-CCSD	1.311	1.096	118.8	29.5	3.70	188
	CIS	1.248	1.087	118.2	22.5	4.51	24
$\tilde{A}^1A_2$ (TS)d	EOM-CCSD	1.314	1.091	123.3	0.0	3.70	
	CIS	1.248	1.084	120.9	0.0	4.51	
1^1B_1	EOM-CCSD	1.459	1.094	119.4	43.5	8.02	1775
($^1A'$, $\pi^* \leftarrow n_z$)	CIS	1.487	1.079	123.0	49.4	8.13	1385
$^{11}B_1$ (TS)[d]	EOM-CCSD	1.430	1.084	137.2	0.0	8.24	
	CIS	1.481	1.069	142.6	0.0	8.30	
$\tilde{B}^1A_1$	EOM-CCSD	1.583	1.095	118.5	0.0	8.43	
($\pi^* \leftarrow \pi$)	CIS	1.455	1.075	124.4	0.0	8.62	
$\tilde{C}^1B_2$	EOM-CCSD	1.198	1.131	120.7	0.0	7.06	
(3s $\leftarrow n_y$)	CIS	1.124	1.181	101.0	0.0	7.81	
$\tilde{X}^2B_2$ (radical	UCCSD	1.198	1.115	120.3	0.0		
cation)	UHF	1.204	1.092	118.0	0.0		

[a] Out-of-plane bending angle. [b] Adiabatic transition energy. [c] Inversion barrier. [d] Transition state for inversion of pyramidal geometry.

given in Table 3. EOM-CCSD gives a barrier (188 cm^{-1}) in reasonable agreement with the experimental value (∼316 cm^{-1}), but CIS gives a much smaller barrier.

The origin of the change in geometry with respect to the ground state is also of interest. The π orbital has the larger coefficient at oxygen because of its higher electronegativity as compared to carbon. As a result, the π^* orbital has the larger coefficient at carbon.[21] Thus, a $\pi^* \leftarrow n_y$ transition would lead to the transfer of electron density from the oxygen lone pair to the carbonyl carbon, making the carbon effectively four-coordinate and leading to pyramidalization. This suggestion can be checked by examining the change in charge density on going from the ground state to the relaxed excited state. The change in charge density for the vertical $\pi^* \leftarrow n_y$ state has been examined by Streitwieser and Kohler using projection density plots,[21] and an electron localization function (ELF)[17] analysis has been carried out for the vertical $\pi^* \leftarrow n$ state of a related compound, acetone.[22] However, the charge distributions for the adiabatic excited states have not been examined.

The change in charge density would in any case be small compared to the total charge density. With vertical excited states, the change can be examined by the use of charge density difference plots.[23] However, the change in geometry on going to the adiabatic excited state precludes the use of these plots. As an alterative, one can examine deformation density[24] plots in which the charge distributions for spherically symmetrical neutral atoms at the appropriate nuclear positions are subtracted from the total charge density.

The CIS calculations readily allow the natural orbitals for the excited state to be obtained so that the charge distributions can be calculated. The relaxed natural orbitals for the EOM-CCSD calculations can also be obtained. Figure 2 shows the deformation density plots derived from the EOM-CCSD natural orbitals. The first plot (a) is for the formaldehyde ground state, the second plot (b) is for the planar transition state for the inversion of the relaxed $n\pi^*$ excited state, and the third plot (c) is for the relaxed excited state. These plots have the molecule in the plane of the paper, and plot d corresponds to plot c with the molecule rotated by 90°.

The blue contours indicate regions that have gained charge density with respect to the isolated atoms, and the red regions show depletion. The depletion region near the oxygen in Figure 2a indicates that the carbonyl oxygen has a somewhat more diffuse charge density than for the reference neutral oxygen atom. In the ground state, charge density is transferred from carbon to oxygen in accord with the difference in electronegativity, and the density associated with the hydrogens is polarized toward the carbon. On going to the excited state, the in-plane lone pair loses charge density, and it is transferred to the methylene group. The planar transition state (Figure 2b) for inverting the pyramidal adiabatic structure has a deformation density similar to that of the vertical excited state, but when it is allowed to pyramidalize, out-of-plane charge density appears at carbon, as can be seen in plots 2c and 2d.

An electron localization function (ELF) analysis[17] of the adiabatic excited states was also carried out so that the two methods of examining the charge density distribution could be compared. In this procedure, a topological analysis is carried out to partition the molecular space into basins. The quantity η is defined so that it takes the value of 1.0 for complete localization and 0.0 for complete delocalization.

Figure 3 shows the ELF plots for the $\pi^* \leftarrow n_y$ excited state using a fixed value of η. Here, plot a is for the ground state, plot b is for the vertical excited state, plot c is for the transition state for the inversion of the adiabatic excited state, and plot d is for the relaxed excited state. The lower plots give the 90°-rotated views.

The hydrogens are relatively loosely bound, have large contours, and are shown in turquoise. In plot a, the strongly localized core carbon and oxygen electrons are shown as blue and red dots. The more delocalized lone pairs at oxygen have larger contours and are shown in green/orange. On going to the excited state, charge density is transferred from oxygen to carbon, and the lone-pair electrons are more delocalized. Finally, in the adiabatic structure, there is a feature corresponding to the asymmetric charge distribution at carbon in Figure 2d.

The $\pi^* \leftarrow n_z$ transition (A') was examined in the same fashion. It has a much higher energy, and although it has not been studied experimentally, the calculations find it to be significantly more bent than the $\pi^* \leftarrow n_y$ excited state. Figure 4 shows the deformation density. Plot a shows the B_1 vertical state, plot b shows the planar relaxed transition state between the adiabatic states, and plot c shows the adiabatic state. Here, charge is transferred from the lone pair along the C−O axis to the carbon and the hydrogens. Relaxation to the planar structure in b leads to some shift in charge density, and

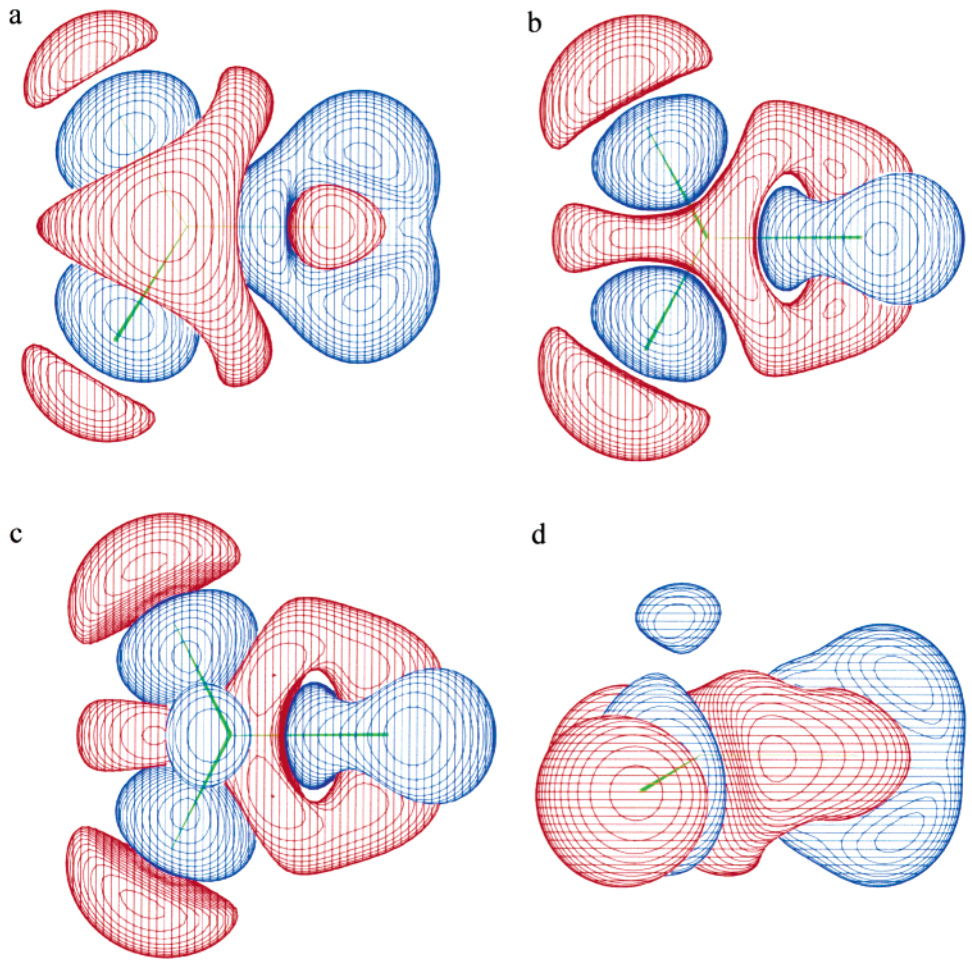

Figure 2. Deformation density plots for the $\tilde{A}^1A_2$ ($\pi^* \leftarrow n_y$) adiabatic excited state for formaldehyde. The blue contours indicate regions that have gained charge density with respect to the neutral atoms, and the red regions show charge depletion. (a) Formaldehyde ground state, (b) planar transition state for the inversion of the relaxed excited state, (c) relaxed excited state, and (d) same as c except rotated by 90°.

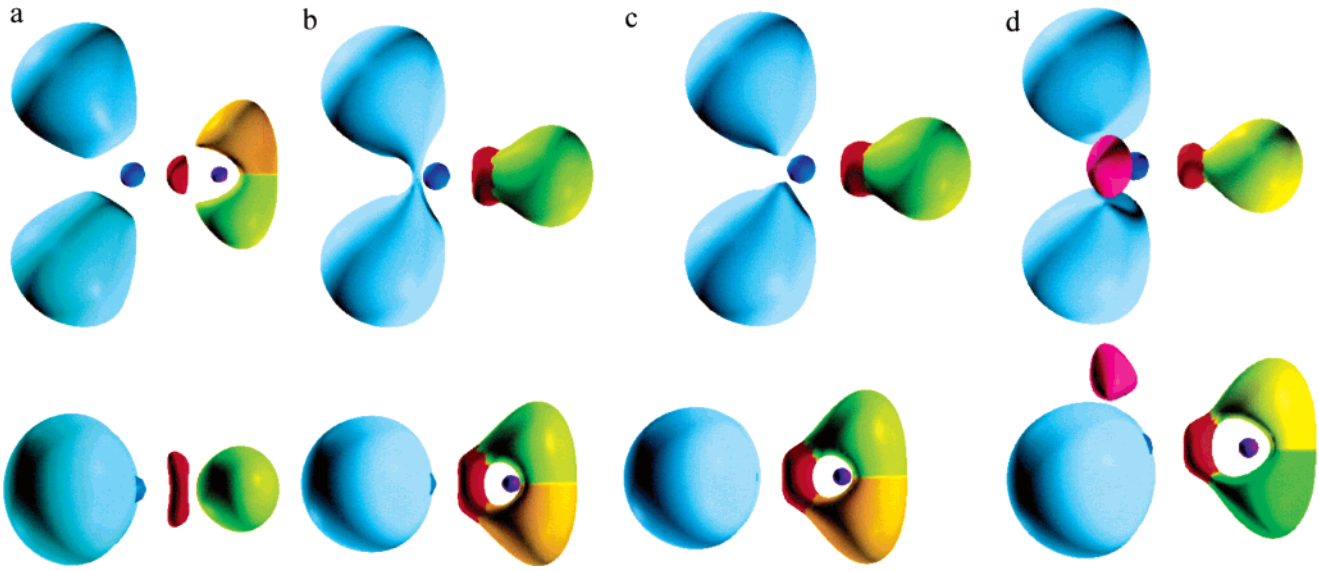

Figure 3. ELF plots for the $\tilde{A}^1A_2$ ($\pi^* \leftarrow n_y$) excited state for formaldehyde. (a) Ground state, (b) vertical excited state, (c) transition state for inversion of the adiabatic excited state, and (d) relaxed excited state. The lower plots give the 90°-rotated views.

relaxation to the adiabatic geometry leads to further shifts in charge density and an out-of-plane charge distribution as seen in plots c and d.

The lowest-energy Rydberg state (3s $\leftarrow n_y$, B_2) was also examined. The CIS- and EOM-CCSD-predicted structures are compared in Table 3 and are in fairly good agreement. The C═O bond length is somewhat decreased, and this state is predicted to have a planar geometry. It might be expected to have a geometry similar to that of the lowest-energy radical cation, and Table 3 shows that this expectation is realized.

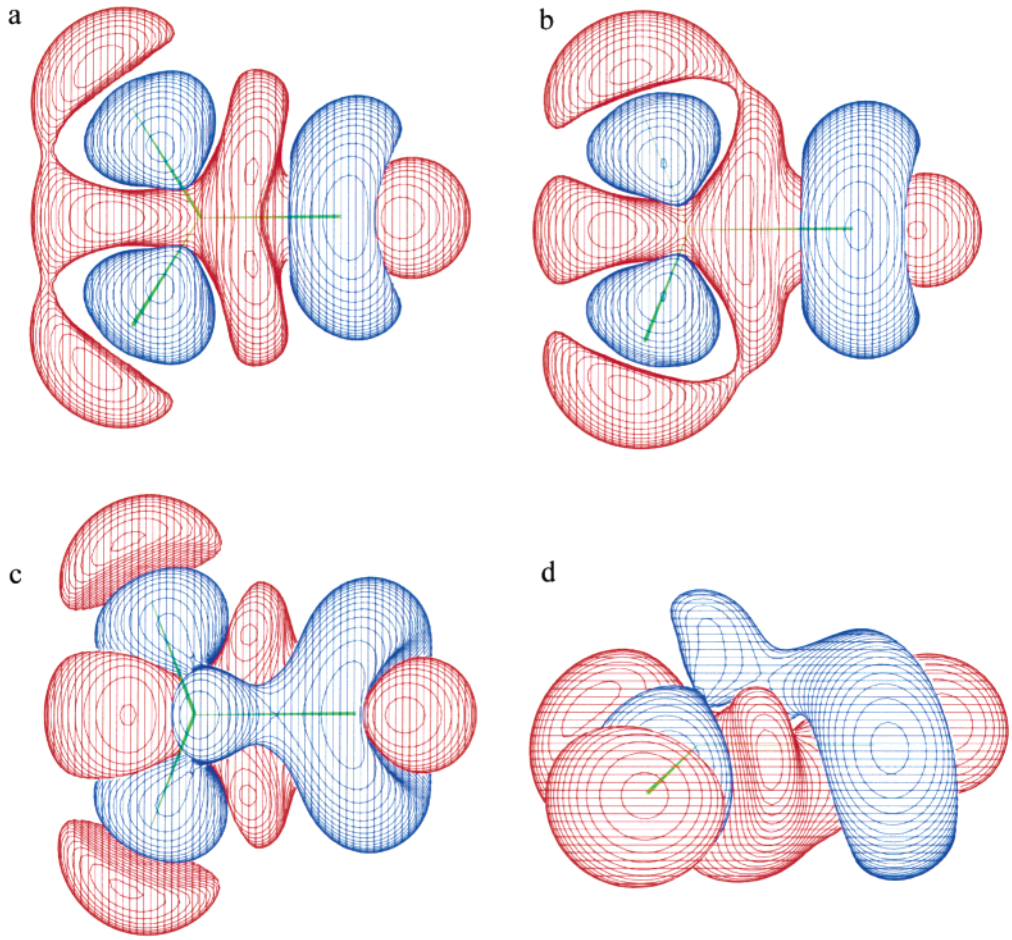

Figure 4. Deformation density plots for the 1 $^1B_1$ ($\pi^* \leftarrow n_z$) adiabatic excited state for formaldehyde. (a) Vertical excited state, (b) transition state for the inversion of the adiabatic excited state, (c) relaxed excited state, and (d) same as c except rotated by 90°.

TABLE 4: Calculated and Observed Relaxed Structures for Thioformaldehyde Excited States

state	level	r(C═S) (Å)	r(C−H) (Å)	∠HCH (deg)	α[a]	TE[b] (eV)	barrier[c] (cm^{-1})
$\tilde{X}^1A_1$ (GS)	expt[26]	1.614	1.096	116.2	0.0		
	CCSD (full)	1.615	1.091	115.9	0.0		
	HF	1.596	1.080	115.9	0.0		
$\tilde{A}^1A_2$	expt[19]	1.682	1.077	120.7	0.0	2.04[d]	
($\pi^* \leftarrow n_y$)	EOM-CCSD	1.698	1.087	119.7	0.0	2.20	
	CIS	1.637	1.077	118.3	0.0	2.68	
1^1B_1	EOM-CCSD	1.936	1.094	115.3	35.1	6.03	3442
($^1A'$,$\pi^* \leftarrow n_z$)	CIS	1.919	1.082	117.3	46.9	5.71	2792
1^1B_1 (TS)	EOM-CCSD	1.844	1.085	138.9	0.0	6.46	
	CIS	1.933	1.069	146.2	0.0	6.05	

[a] Out-of-plane bending angle. [b] Adiabatic transition energy. [c] Inversion barrier. [d] Judge, R. H.; King, G. W. *J. Mol. Spectrosc.* **1979**, *74*, 175.

5. Thioformaldehyde

Whereas the $\pi^* \leftarrow n_y$ state of formaldehyde is pyramidal, the corresponding state of thioformaldehyde is planar.[18] The difference probably is due to the difference in electronegativity between oxygen and sulfur. Whereas the π^* orbital of formaldehyde has the larger coefficient at carbon, the similar electronegativities of carbon and sulfur lead to approximately equal but opposite coefficients at the two atoms of the π^* orbital of thioformaldehyde.[25] Thus, donation of charge density from the sulfur lone pair appears in the C═S bond rather than mainly at the carbon as in formaldehyde.

The results of calculations for thioformaldehyde are reported in Table 4. The CCSD geometry optimization for the ground state gives bond lengths in very good agreement with the experimental values.[26] The HF geometry is fairly good, with a slightly short C═S bond.

The A″ $\pi^* \leftarrow n_y$ transition is calculated to lead to a planar relaxed structure, and the EOM-CCSD geometry and excitation energy are in very good agreement with the experimental results. The CIS results are also in agreement with the experiments. It should be noted that, even though the relaxed structure is planar, a transition to this structure is electronically forbidden. Thus, the observed transition is to a vibronically distorted structure that then relaxes to the observed structure. The deformation density plots for the ground state and this excited state are shown in Figure 5. The similarity with formaldehyde readily is apparent.

The A′ $\pi^* \leftarrow n_z$ excited state is calculated to be pyramidal and thus is similar to the corresponding excited state of

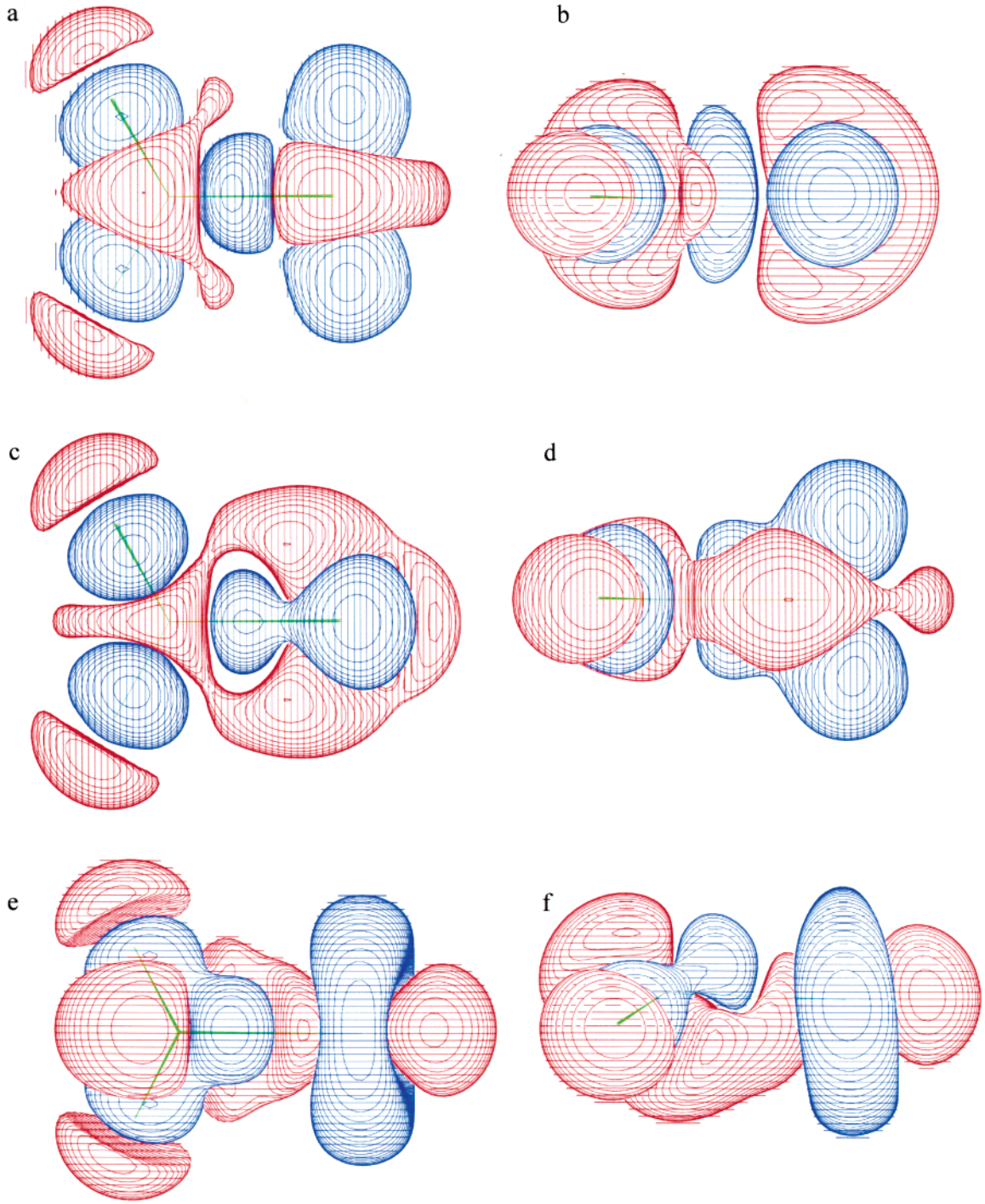

Figure 5. Deformation density plots for thioformaldehyde: (a) $\tilde{X}^1A_1$ ground state, (b) $\tilde{X}^1A_1$ ground state rotated by 90°, (c) $\tilde{A}^1A_2$ ($\pi \leftarrow n_y$) excited state, (d) $\tilde{A}^1A_2$ ($\pi \leftarrow n_y$) excited state rotated by 90°, (e) 1^1B_1 ($\pi^* \leftarrow n_y$) excited state; (f) 1^1B_1 ($\pi^* \leftarrow n_y$) excited state rotated by 90°.

formaldehyde. No experimental are available data for the adiabatic state. The CIS calculation gives a similar geometry, but here, the C═S bond is calculated to be significantly longer than in the EOM-CCSD structure. The deformation density plots for this state are shown in Figure 5. Again, this state is quite similar to the corresponding formaldehyde excited state. There appears to be a larger degree of charge transfer in the A′ state than in A″, and this is probably the origin of its pyramidalized structure.

6. Carbon Disulfide

The complex near-ultraviolet spectrum of carbon disulfide long has been attributed to valence $\pi^* \leftarrow \pi$ transitions involving low-lying $(2\pi_g)^3(3\pi_u)^1$ electronic configurations of the linear molecule. This rudimentary description gives rise to singlet and triplet manifolds of closely spaced Σ_u^+, Δ_u, and Σ_u^- levels, leading to eight excited states of bent equilibrium geometry that can interact through a variety of mechanisms. The reduction in symmetry accompanying distortion of the molecular framework from linearity ($D_{\infty h} \rightarrow C_{2v}$) demands that states of Σ_u^+ and Σ_u^- parentage be correlated uniquely to B_2 and A_2 irreducible representations, respectively. In a similar fashion, the doubly degenerate Δ_u levels can be resolved into B_2 and A_2 components, which, as a result of vibronic interactions associated with the Renner−Teller effect,[27] exhibit distinct (nondegenerate) electronic energies for all values of the bending angle other than $\theta_{SCS} = 180°$.

TABLE 5: Calculated and Observed Structures for Carbon Disulfide Singlet States

state	level	r(C−S) (Å)	∠S−C−S (deg)	TE[a] (eV)	barrier[b] (cm^{-1})
$\tilde{X}^1\Sigma_g^+$ (GS)	expt[c]	1.556	180	−	−
	CCSD (full)	1.557	180	−	−
	HF	1.543	180	−	−
$\tilde{A}^1A_2$ ($^1\Sigma_u^-$)	expt[d]	−	135	3.64	2800
	EOM-CCSD	1.633	138.4	3.45	3563
	CIS	1.600	142.2	3.96	1716
$^1\Sigma_u^-$ (TS)	EOM-CCSD	1.614	180	3.89	−
	CIS	1.579	180	4.17	−
$\tilde{B}^1B_2$ ($^1\Delta_u$)	expt[e]	1.64	131.9	3.50	3681
	EOM-CCSD	1.634	131.9	3.64	2286
	CIS	1.616	144.5	4.29	447
$\tilde{C}^1A_2$ ($^1\Delta_u$)	expt[e]	1.64	174	3.96	75
	EOM-CCSD	1.616	175.6	3.92	19
	CIS	1.579	173.6	4.34	14
$^1\Delta_u$ (TS)	EOM-CCSD	1.616	180	3.92	−
	CIS	1.579	180	4.34	−

[a] Adiabatic transition energy. [b] Barrier to linearity. [c] Smith, D. F. J.; Overend, J. *J. Chem. Phys.* **1971**, *54*, 3632. [d] Jungen, C.; Malm, D. N.; Merer, A. J. *Can. J. Phys.* **1973**, *51*, 1471. [e] Brasen, G.; Leidecker, M.; Demtröder, W.; Shimámoto, T.; Katô, H. *J. Chem. Phys.* **1998**, *109*, 2779.

Several quantum chemistry studies have been reported for the $\pi^*\pi$ excited states of carbon disulfide.[28−32] The most comprehensive of these prior efforts are the CIS/6-311+G* and CIS-MP2/6-311+G* analyses of Zhang and Vaccaro,[30] which examined the electronic energies, equilibrium geometries, transition strengths, and barrier heights to linearity, as well as isotopomer-specific rotational and vibrational constants, for the lowest-lying manifolds of singlet and triplet multiplicity. In particular, these authors predicted a relative ordering of bent excited states and accompanying correlation to linear parentage that differed markedly from the patterns deduced by earlier spectroscopic measurements. Subsequent Doppler-free laser-induced fluorescence work conducted under rovibonically cold molecular beam conditions corroborated many of these theoretical assertions,[31] including identification of the strongly bent V^1B_2 excited state as the lower member of the $^1\Delta_u$ Renner−Teller doublet. Shortly thereafter, Brown, et al.[32] performed analogous ab initio investigations at the substantial CISTDQ and EOM-CCSD levels of theory through use of DZP and TZ2P(f) basis sets. Although agreeing with most of the CIS results deduced by Zhang and Vaccaro, these higher-level calculations predicted transition energies in much better accord with experimental findings and suggested (at the most substantial levels of theory) that the bent equilibrium geometry for the $\tilde{C}^3B_2$ ($^3\Delta_u$) triplet manifold should reside below that for the neighboring $\tilde{B}^1B_2$ ($^1\Delta_u$) singlet state.

Table 5 compares structural parameters (r_{CS} and θ_{SCS}), transition energies, and (where appropriate) barriers to linearity determined experimentally for the lowest-lying singlet manifolds of CS_2 with analogous ab initio quantities extracted from fully relaxed (optimized) configurations of the S−C−S nuclear framework. In particular, our quantum chemistry calculations have exploited various levels of theory in conjunction with the substantial 6-311++G** basis set to examine minimum-energy and transition-state geometries for each potential energy surface. The linear equilibrium structure of the $\tilde{X}^1\Sigma_g^+$ ground electronic state is found to be reproduced quantitatively by the CCSD treatment while the less aggressive HF approach yields only a 0.013 Å discrepancy between measured and calculated values of the C−S bond length.

The excited singlet states of CS_2 examined in the present study are theoretically predicted and experimentally found to support symmetrically bent equilibrium structures that exhibit substantial elongation of the C−S bonds relative to the $\tilde{X}^1\Sigma_g^+$ ground-state value of 1.5562 Å.[33] Although the latter observation is in keeping with the reduction in bond strength expected to accompany the $\pi^* \leftarrow \pi$ electron promotion process, the corresponding distortion of the molecular framework from linearity can be rationalized through Walsh-type arguments that show the $9a_1^*$ component of the excited $3\pi_u^*$ molecular orbital to energetically favor bent configurations. In all cases, EOM-CCSD structural parameters and transition energies are in much better agreement with laboratory measurements than their CIS counterparts. This is especially true for the $\tilde{B}^1B_2$ and $\tilde{C}^1A_2$ manifolds, which constitute the lower-lying and higher-lying members of the $^1\Delta_u$ Renner−Teller doublet, respectively, where EOM-CCSD predictions reproduce results deduced from recent spectroscopic analyses in a near-quantitative fashion. Barrier heights, calculated as the difference in energy between relaxed geometries for the bent (minimum-energy) and linear (transition-state) configurations of each state, are in reasonable accord with experimental findings given the small magnitude of such quantities.

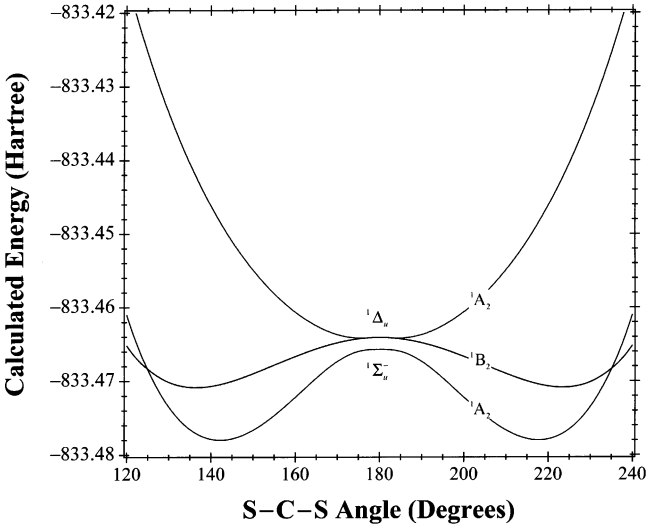

Figure 6. Electronic potential curves for CS_2 as a function of S−C−S angle. The dependence of CS_2 electronic energy on the S−C−S bending coordinate is calculated at the EOM-CCSD/6-311++G** level of theory for a fixed value of the common C−S bond distance (r_{CS} = 1.56 Å). Symmetry labels are affixed to each potential curve with correlations between linear and bent structures indicated explicitly.

Figure 6 depicts CS_2 bending potentials calculated at the EOM-CCSD/6-311++G** level of theory by fixing the two C−S bond lengths at the common value of r_{CS} = 1.56 Å and varying the S−C−S bond angle over the range 120° ≤ θ_{SCS} ≤ 240°. As highlighted by these curves and reinforced by the relaxed-geometry data compiled in Table 6, the lowest-lying singlet electronic states are predicted to exhibit an energy ordering of the form

$$\tilde{X}^1\Sigma_g^+ < \tilde{A}^1A_2\,(^1\Sigma_u^-) < \tilde{B}^1B_2\,(^1\Delta_u) < \tilde{C}^1A_2\,(^1\Delta_u)$$

The resulting correlation of the $\tilde{C}^1A_2$ and $\tilde{B}^1B_2$ curves as the upper and lower members of the $^1\Delta_u$ Renner−Teller doublet is the inverse of that suggested by early spectroscopic analyses; however, more recent high-resolution studies by Brasen et al.[31] have provided unequivocal support for our ab initio ordering of levels. Such behavior can be justified from the viewpoint of symmetry-conserving electronic perturbations, whereby repulsive interaction between the $^1A_2$ ($^1\Sigma_u^-$) and $^1A_2$ ($^1\Delta_u$) surfaces

TABLE 6: Calculated and Observed Structures for Carbon Dioxide Singlet States

state	level	r(C−O) (Å)	∠O−C−O (deg)	TE[a] (eV)	barrier[b] (cm^{-1})
$\tilde{X}^1\Sigma_g+$ (GS)	expt[c]	1.162	180	–	–
	CCSD (full)	1.160	180	–	–
	HF	1.136	180	–	–
$\tilde{A}^1A_2$ ($^1\Sigma_u^-$)	EOM-CCSD	1.242	129.1	5.68	20089
	CIS	1.210	130.3	6.85	12949
$^1\Sigma_u^-$ (TS)	EOM-CCSD	1.265	180	8.17	–
	CIS	1.219	180	8.45	–
$\tilde{B}^1B_2$ ($^1\Delta_u$)	expt[c]	1.246	122.0	5.8[d]	
	EOM-CCSD	1.238	120.9	5.81	19500
	CIS	1.210	124.4	7.35	17000
$\tilde{C}^1A_2$ ($^1\Delta_u$)	EOM-CCSD	1.266	176.0	8.20	147
	CIS	1.229	174.1	9.39	470
$^1\Delta_u$ (TS)	EOM-CCSD	1.267	180	8.22	–
	CIS	1.218	180	9.46	–
$\tilde{D}^1B_2$ ($^1\Pi_g$)	EOM-CCSD	1.167	180	11.36	–
	CIS	1.165	180	10.15	–
$\tilde{E}^1A_2$ ($^1\Pi_g$)	EOM-CCSD	1.168	180	11.44	–
	CIS	1.165	180	10.15	–

[a] Adiabatic transition energy. [b] Barrier to linearity. [c] Herzberg, G. *Electronic Spectra of Polyatomic Molecules*, New York, VanNostrand Reinhold Co. 1966. [d] Dixon, R. N. *Discuss. Farad. Soc.* **1963**, *35*, 105.

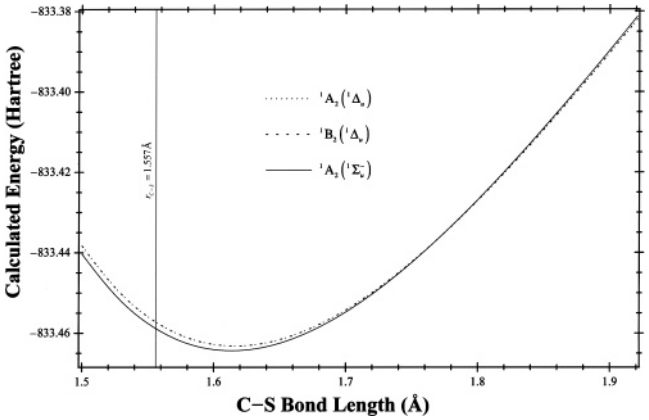

Figure 7. Electronic potential curves for CS_2 as a function of C−S distance. The dependence of CS_2 electronic energy on the common C−S stretching coordinate is calculated at the EOM-CCSD/6-311++G** level of theory for a near-linear (θ_{SCS} = 179.99°) configuration of the molecular framework. Dashed curves denote the $^1A_2$ and $^1B_2$ Renner−Teller components emerging from the $^1\Delta_u$ manifold, and the solid curve represents the neighboring $^1A_2$ state of $^1\Sigma_u^-$ parentage. A crossing between the $^1\Delta_u$ and $^1\Sigma_u^-$ potential curves is predicted to occur at C−S bond distances of ∼1.78 Å.

pushes the latter above its $^1B_2$ ($^1\Delta_u$) sibling. Clearly, the validity of this argument hinges on the proximate $^1\Sigma_u^-$ state residing *below* the $^1\Delta_u$ manifold. Figure 7 shows EOM-CCSD/6-311++G** potential curves calculated as a function of the common C−S bond length for a slight (0.01°) distortion of the molecular framework from linearity, thereby yielding essentially degenerate $^1A_2$ and $^1B_2$ states of $^1\Delta_u$ parentage. Whereas the $^1\Sigma_u^-$ state is predicted to lie below the $^1\Delta_u$ manifold for r_{CS} values comparable to those encountered in the pertinent equilibrium geometries (cf. Table 5), this situation found to be reversed for C−S bond lengths in excess of ∼1.775 Å.

7. Carbon Dioxide

Although carbon disulfide and carbon dioxide are isovalent, the reduced number of total electrons in the latter species ostensibly should make the reliable ab initio prediction of electronic energies and equilibrium geometries a less formidable task. This situation is complicated by the high-lying nature of the $(1\pi_g)^3(2\pi_u)^1$ valence states in CO_2 that places them in proximity to Rydberg features of nominal $(1\pi_g)^3(3s\sigma_g)^1$ and $(1\pi_g)^3(3p\pi_u)^1$ parentage. Whereas the $(1\pi_g)^3(3s\sigma_g)^1$ configuration gives rise to singlet and triplet Π_g Rydberg manifolds that each correlate to A_2 and B_2 components upon distortion from linearity, the $(1\pi_g)^3(3p\pi_u)^1$ configuration leads to Σ_u^+, Δ_u, and Σ_u^- Rydberg levels analogous to those resulting from the valence $(1\pi_g)^3(2\pi_u)^1$ configuration. Strong interactions among neighboring excited states, producing numerous and pronounced avoided crossings in the pertinent potential energy surfaces, are expected, with the CO_2^+ ion core of the Rydberg manifolds imposing a partial preference for the linear structure. To date, the most sophisticated theoretical analyses reported for the CO_2 electronic spectrum are the multireference single- and double-excitation configuration interaction (MRD-CI with 10 active electrons) calculations of Buenker and co-workers.[34] Geometry optimizations were not attempted in this study; however, these authors did examine the relevant bending potential curves and accompanying generalized oscillator strengths (from the $\tilde{X}^1\Sigma_g^+$ ground electronic state) for transitions residing below ∼13 eV.

Table 6 presents a compilation of ab initio results obtained for the lowest-lying singlet manifolds of CO_2 by examining both minimum-energy (fully relaxed) and transition-state configurations of the O−C−O nuclear framework. The tabulated structural parameters (r_{CO} and θ_{OCO}), transition energies, and (where appropriate) barriers to linearity were calculated through use of the substantial 6-311++G** basis set and have been compared to available experimental data. The linear equilibrium geometry for the $\tilde{X}^1\Sigma_g^+$ ground electronic potential surface is found to be reproduced quantitatively by the CCSD level of theory, and analogous HF predictions underestimate the C−O bond length by only 0.026 Å.

As expected by the attendant removal of electron density from the bonding $1\pi_g$ molecular orbital, all of the low-lying excited singlet states of CO_2 support symmetrical minimum-energy structures (C_{2v} or $D_{\infty h}$) that entail substantial elongation of the C−O bond relative to the $\tilde{X}^1\Sigma_g^+$ (ground state) value of 1.162 Å. This has a profound influence on the ordering and shape of electronic manifolds, a fact highlighted by Figure 8, which contrasts bending potential curves calculated at the EOM-CCSD/6-311++G** level of theory by fixing the common C−O bond length to (a) r_{CO} = 1.16 Å (essentially the ground-state value) and (b) r_{CO} = 1.24 Å (a value in keeping with excited-state equilibrium structures). The three pertinent electronic states found at the linear configuration (θ_{OCO} = 180°),$^1\Sigma_u^-$, $^1\Delta_u$, and $^1\Pi_g$, should not interact strongly under the auspices of symmetry- and spin-conserving perturbations as long as the molecular framework retains strict linearity. The top panel in Figure 8 shows that the energy ordering of linear states for r_{CO} parameters close to those encountered in the $\tilde{X}^1\Sigma_g^+$ equilibrium geometry has the form

$$^1\Delta_u > {}^1\Sigma_u^- > {}^1\Pi_g$$

where the $^1\Pi_g$ manifold can be correlated unambiguously to the $(1\pi_g)^3(3s\sigma_g)^1$ Rydberg configuration, and examination of density difference plots for the $^1\Sigma_u^-$ and $^1\Delta_u$ potential surfaces suggests that they stem from the $(1\pi_g)^3(2\pi_u)^1$ valence configuration. Stretching of the common C−O bond length causes a precipitous drop in energy for the $^1\Sigma_u^-$ and $^1\Delta_u$ states, with the energy of the $^1\Pi_g$ manifold found to rise by a comparable amount. As depicted in the lower panel of Figure 8, these

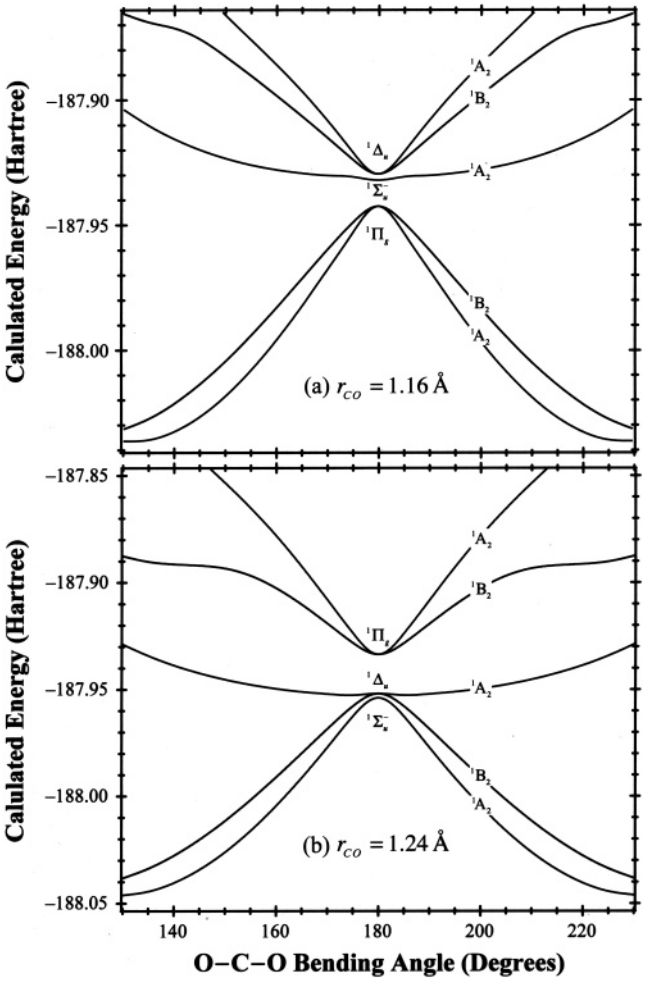

Figure 8. Electronic potential curves for CO_2 as a function of O−C−O angle. The dependence of CO_2 electronic energy on the O−C−O bending coordinate is calculated at the EOM-CCSD/6-311++G** level of theory for two values of the common C−O bond distance, r_{CO} = (a) 1.16 and (b) 1.24 Å, where the former is in keeping with the equilibrium geometry of the $\tilde{X}^1\Sigma_g^+$ ground state and the latter reflects the elongation of C−O bonds accompanying promotion of an electron from the $1\pi_g$ molecular orbital. Symmetry labels are affixed to each potential curve with correlations between linear and bent structures indicated explicitly. The extension of C−O bonds upon electronic excitation leads to a pronounced change in the energy ordering of linear ($D_{\infty h}$) manifolds, as well as a mixing of linear parentage for the emerging bent (C_{2v}) electronic states.

antagonistic effects lead to a partial reversal of the linear state ordering when r_{CO} attains the value of 1.24 Å

$$^1\Pi_g > {}^1\Delta_u > {}^1\Sigma_u^-$$

Distortion of the O−C−O nuclear framework from linearity breaks the degeneracy of the $^1\Pi_g$ and $^1\Delta_u$ manifolds, with the resulting pairs of $^1A_2$ and $^1B_2$ states interacting strongly among themselves as well as with the lone $^1A_2$ state derived from the linear $^1\Sigma_u^-$ manifold. The bending potential curves in Figure 8 show unmistakable signs of avoided crossings; however, the overall trends and patterns can be rationalized qualitatively though use of state repulsion arguments based upon symmetry- and spin-conserving electronic perturbations.

The two panels in Figure 8 demonstrate that the relative energy ordering of $^1A_2$ and $^1B_2$ manifolds in the CO_2 system remains unaltered as the common C−O bond length is stretched from the $\tilde{X}^1\Sigma_g^+$ value of r_{CO} = 1.16 Å; however, the linear parentage and detailed shapes for the emerging potential surfaces

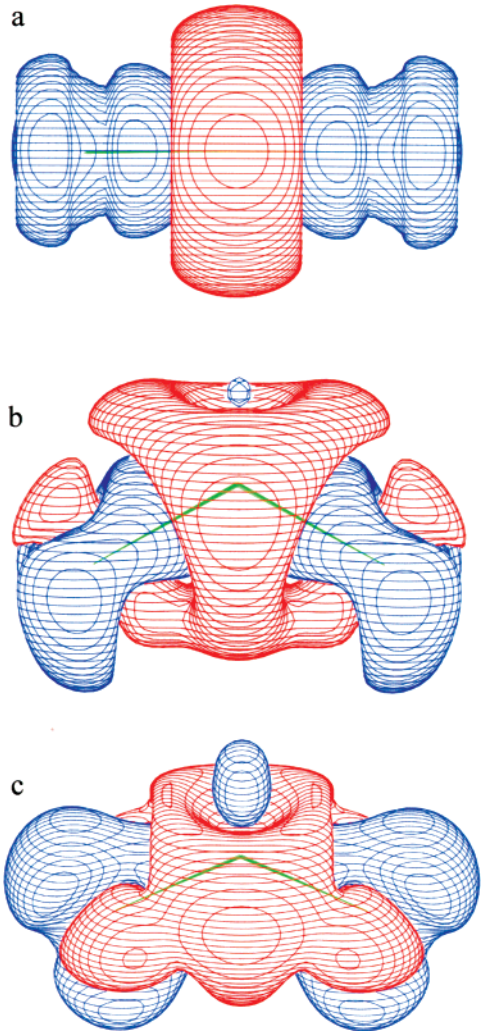

Figure 9. Deformation density plots for carbon dioxide: (a) $\tilde{X}^1\Sigma_g^+$ ground state, (b) $\tilde{B}^1B_2$ ($^1\Delta_u$) excited state, (c) $\tilde{A}^1A_2$ ($^1\Sigma_u^-$) excited state.

are found to change dramatically. The lowest-lying $\tilde{A}^1A_2$ ($^1\Sigma_u^-$) and $\tilde{B}^1B_2$ ($^1\Delta_u$) excited states are predicted to support strongly bent equilibrium structures that exhibit substantial (>2 eV) barriers to linearity, with EOM-CCSD/6-311++G** calculations reproducing available experimental data for the $\tilde{B}^1B_2$ surface in a near-quantitative fashion. The higher-lying $\tilde{C}^1A_2$ ($^1\Delta_u$) manifold represents the upper component of the $^1\Delta_u$ Renner−Teller doublet and is expected to exhibit a minimum-energy configuration that is distorted only slightly from linearity (θ_{OCO} = 176°). The $\tilde{D}^1B_2$ ($^1\Pi_g$) and $\tilde{E}^1A_2$ ($^1\Pi_g$) hypersufaces stem from the $(1\pi_g)^3(3s\sigma_g)^1$ Rydberg configuration and are displaced to substantially higher energies. In keeping with the preferred geometry for the CO_2^+ ion core, these states are predicted to have linear equilibrium structures.

The modifications in electronic charge distribution following excitation from the $\tilde{X}^1\Sigma_g^+$ ground state to the $\tilde{A}^1A_2$ ($^1\Sigma_u^-$) and $\tilde{B}^1B_2$ ($^1\Delta_u$) potential surfaces were examined to elucidate the linear-to-bent nature of the accompanying change in equilibrium geometry. This task was accomplished through use of both deformation densities and the ELF function, with the former being shown in Figure 9 while the latter, as well as ancillary information related to AIM and ELF charge analyses, has been relegated to the compilation of Supporting Information. The $\tilde{X}^1\Sigma_g^+$ deformation density found in panel a demonstrates the polarization of C−O bonds induced by the more electronegative oxygen atoms. The analogous $\tilde{A}^1A_2$ ($^1\Sigma_u^-$) and $\tilde{B}^1B_2$ ($^1\Delta_u$) plots

TABLE 7: Calculated and Observed Relaxed Structures for Sulfur Dioxide Excited States

state	level	r(SO)a (Å)	r(SO)b (Å)	∠O−S−O (deg)	TE[a] (eV)	barrier[b] (cm^{-1})
$\tilde{X}^1A_1$ (GS)	expt[c]	1.431	1.431	119.3		
	CCSD (full)	1.445	1.445	118.8		
	HF	1.408	1.408	118.6		
$\tilde{C}^1B_2$ ($^1A'$)	expt[35]	1.491	1.639		5.28	141
	EOM-CCSD	1.510	1.630	104.9	5.48	19
	CIS	*d*				
$\tilde{C}^1B_2$	EOM-CCSD	1.560	1.560	104.8	5.48	
(TS, C_{2v})	CIS	1.515	1.515	105.3	6.29	

[a] Adiabatic transition energy. [b] Barrier to C_{2v}. [c] Morino, Y.; Tanimoto, M.; Saito, S. *Acta. Chem. Scand. A* **1988**, *42*, 346. [d] Optimizations result in C_{2v} structure.

depicted in panels b and c, respectively, bear a striking resemblance to those obtained from our study of low-lying singlet states in formaldehyde. In particular, a "lone-pair-like" distribution of charge appears on the carbon atom in these excited states, thereby suggesting an incipient rehybridization of the carbon center that promotes bending of the O−C−O nuclear framework.

8. Sulfur Dioxide

In the ground state, SO_2 has equal S−O bond lengths and is bent. The geometry is well reproduced at the CCSD level (Table 7), and HF calculation also leads to a satisfactory bond angle and a somewhat short S−O bond as is characteristic of this level of theory. The $\tilde{C}^1B_2$ excited state has been reported to have a decreased O−S−O bond angle and unequal S−O bond lengths.[35] Both the CIS and EOM-CCSD calculations satisfactorily reproduce the change in bond angle. The CIS calculation leads to equal S−O bond lengths that are somewhat short, as was found with the HF calculation for the ground state. The EOM-CCSD calculation leads to unequal S−O bond lengths in agreement with the more recent experimental structure and gave a transition energy close to the experimental value. However, the structure having equal bond lengths was only slightly higher in energy and the calculated barrier was only 19 cm^{-1} whereas the observed barrier is 141 cm^{-1}. A multireference calculation reproduced both the difference in bond length and the observed barrier.[36]

The deformation density plots for (a) the ground state, (b) the $\tilde{C}^1B_2$ transition state with equal S−O bond lengths, and (c) the adiabatic geometry are shown in Figure 10. The large polarization of the S−O bonds is apparent in the ground state. The change in electron density on going to the excited state (transition state) with equal S−O bond lengths is not obvious in Figure 10b, but an AIM analysis (Supporting Information) shows that about 0.4 electron is transferred from oxygen to sulfur on going to this excited state. There is a further change in electron density distribution on going to the relaxed adiabatic excited state (Figure 10c) and here the AIM analysis suggests a 0.1 electron difference between the two oxygens.

9. Nitrogen Dioxide

Nitrogen dioxide presents additional difficulties with the calculations in that it is a radical. The ground-state geometry[37] is well reproduced at the UHF-CCSD and ROHF-CCSD levels (Table 8). The UHF level gives a satisfactory bond angle but a short N−O bond as is characteristic of this level of theory.

The adiabatic geometry of the $\tilde{A}^2B_2$ has been estimated from laser-induced dispersed fluorescence spectroscopy, and it has an excitation energy of 1.2 eV.[38] The EOM-CCSD and ROHF/

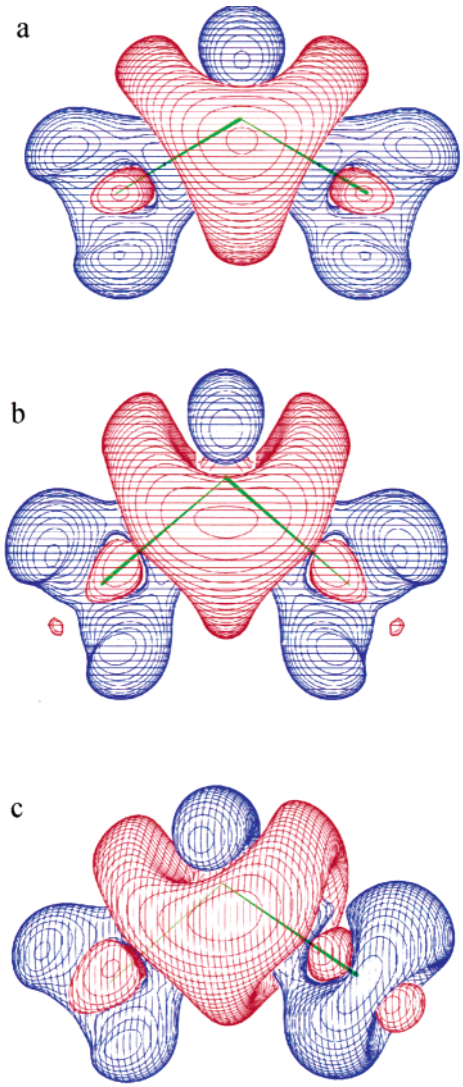

Figure 10. Deformation density plots for sulfur dioxide: (a) $\tilde{X}^1A_1$ ground state, (b) $\tilde{C}^1B_2$ (C_{2v}) excited state with equal S−O bond length, (c) $\tilde{C}^1B_2$ ($^1A'$) adiabatic geometry with unequal S−O bond lengths.

TABLE 8: Calculated and Observed Relaxed Structures for Nitrogen Dioxide Excited States

state	level	r(NO) (Å)	∠O−N−O (deg)	TE[a] (eV)
$\tilde{X}^2A_1$ (GS)	expt[37]	1.194	133.9	
	UHF-CCSD	1.189	134.4	
	ROHF-CCSD	1.189	134.8	
	UHF	1.156	136.4	
$\tilde{A}^2B_2$	expt[38]	1.244	102.6	1.21
	UHF/EOM-CCSD	1.250	102.8	1.23
	ROHF/EOM-CCSD	1.249	102.9	1.226
	UCIS	1.227	101.3	1.305
$\tilde{C}^2A_2$	expt[40]	1.339	108.4	2.01
	UHF/EOM-CCSD	1.265	110.2	2.13
	ROHF/EOM-CCSD	1.263	110.4	2.11
	UCIS	1.231	109.3	1.49

[a] Adiabatic transition energy.

EOM-CCSD levels give essentially the same geometry and an excitation energy that agrees with the experiment. They are also in good agreement with other recent calculations.[39] The UCIS calculation reproduces the change in bond angle on going to this excited state and again gives a somewhat short NO bond length. The difference with respect to the CCSD calculations is essentially the same as found with the ground state.

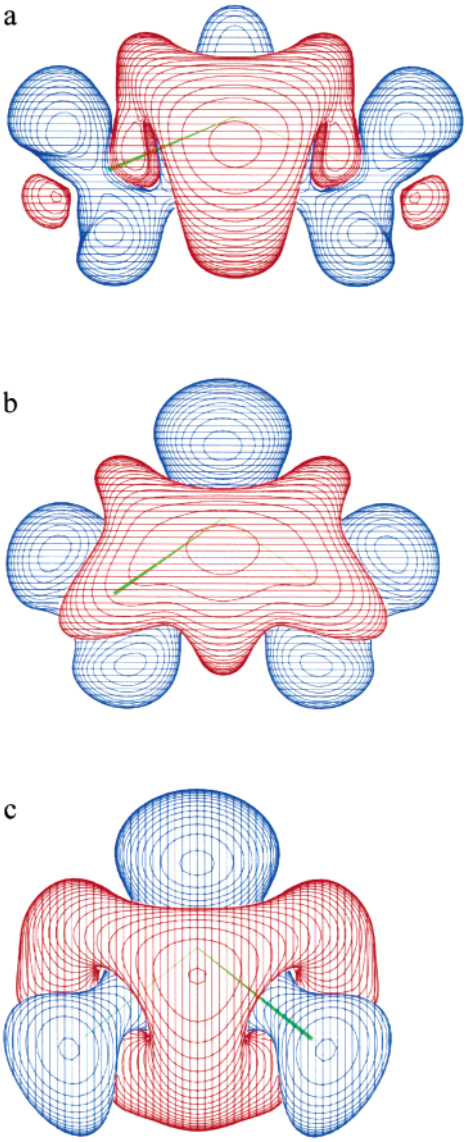

Figure 11. Deformation density plots for carbon dioxide: (a) $\tilde{X}^2A_1$ ground state, (b) $\tilde{A}^2B_2$ excited state calculated at CIS level, (c) $\tilde{C}^2A_2$ excited state calculated at CIS level.

The $\tilde{C}^2A_2$ excited state was also examined, and here there is an experimental geometry.[40] A detailed theoretical study at the CCSD level led to the conclusion that the correct NO bond lengths are significantly less than that inferred from the experiments and led to r(NO) ≈ 1.27Å.[41] All three theoretical levels give a bond angle that is in satisfactory agreement with the experimental value but give bond lengths somewhat less than the experimental value. The EOM-CCSD adiabatic excitation energies are in good agreement with the experimental value.

The deformation densities for the (a) ground state and (b,c) two excited states are shown in Figure 11. The ground-state deformation density is based on CCSD wave functions, but there was difficulty in obtaining the natural orbitals for the excited states from the CCSD-EOM calculations, and therefore, the CIS wave functions were used for the excited states.

Conclusions

The CIS-optimized geometries for the adiabatic excited states of the molecules examined in this study are usually close to those obtained using EOM-CCSD. The latter, in all cases, gave structural parameters that agree well with those obtained in experimental studies. The origin of the changes in structure on going from the ground state to the adiabatic excited states often can be understood by examining deformation density plots that show the change in electron density with respect to spherically symmetrical neutral atoms.

Calculations

The ground-state geometries were calculated using Gaussian 03.[42] The EOM-CCSD excited states were calculated using ACES II[43] and PSI3.[44] A modification of ACES II allowed the program to print natural orbitals corresponding to the relaxed density for the excited states. These natural orbitals were used to replace the MO coefficients in Gaussian formatted checkpoint files, and the rearchive procedure was used to rewrite the natural orbitals on the basis of primitive basis functions in a .wfn file similar to that produced by a Gaussian CIS calculation. The deformation density figures were drawn using CASGEN[45] making use of the .wfn files.

Acknowledgment. This investigation was supported by National Science Foundation Grant CHE-0132678.

Supporting Information Available: Table giving the calculated total energies for all of the states. Tables giving AIM and ELF analyses of the excited states. Figures showing ELF plots for the excited states. This material is available free of charge via the Internet at http://pubs.acs.org.

References and Notes

(1) Jensen, F.; Bunker, P. R. *J. Mol. Spectrosc.* **1982**, *94*, 114.
(2) King, G. W.; Ingold, C. K. *Nature* **1952**, *169*, 1101. Ingold, C. K. *J. Chem. Soc.* **1953**, 2702. Innes, K. K. *J. Chem. Phys.* **1954**, *22*, 863. Foo, P. D.; Innes, K. K. *Chem. Phys. Lett.* **1973**, *18*, 601. Huet, T. R.; Godefroid, M.; Herman, M. J. *J. Mol. Spectrosc.* **1990**, *144*, 32.
(3) Foresman, J. B.; Head-Gordon, M.; Pople, J. A.; Frisch, M. J. *J. Phys. Chem.* **1992**, *96*, 135−149.
(4) Stanton, J. F.; Bartlett, R. J. *J. Chem. Phys.* **1993**, *98*, 7029−7039.
(5) Cf. Hadad, C. M.; Foresman, J. B.; Wiberg, K. B. *J. Phys. Chem.* **1993**, *97*, 4293.
(6) Bartlett, R. J.; Stanton, J. F. In *Reviews in Computational Chemistry*; Lipkowitz, K. B., Boyd, D. B., Eds.: VCH Publishers: New York, 1994; Vol. 5, p 65.
(7) Wiberg, K. B.; Oliviera, A. E.; Trucks, G. *J. Phys. Chem. A* **2002**, *106*, 4192.
(8) Wiberg, K. B. *J. Comput. Chem.* **2004**, *25*, 1342.
(9) Harmony, M. D. *J. Chem. Phys.* **1990**, *93*, 7522 (cf. Berry, R. J.; Harmony, M. D. *Struct. Chem.* **1990**, *1*, 49).
(10) Pawlowski, F.; Jorgensen, P.; Olsen, J.; Hegelund, F.; Helgaker, T.; Gauss, J.; Bak, K. L.; Stanton, J. F. *J. Chem. Phys.* **2002**, *116*, 6482.
(11) The experimental data have been summarized in ref 7. The excited-state calculations have also been summarized in this reference.
(12) Foo, P. D.; Innes, K. K *J. Chem. Phys.* **1974**, *60*, 4582.
(13) Hehre, W. J.; Radom, L.; Schleyer, P. v. R.; Pople, J. A. *Ab Initio Molecular Orbital Theory*; Wiley: New York, 1986.
(14) Sherrill, C. D.; Byrd, E. F. C.; Head-Gordon, M. *J. Chem. Phys.* **2000**, *113*, 1447. Ventura, E.; Dallos, M.; Lischka, H. *J. Chem. Phys.* **2003**, *118*, 1702.
(15) Herman, M.; Colin, R. *Bull. Soc. Chim. Belg.* **1980**, *89*, 335.
(16) Bader, R. F. W. *Atoms in Molecules*; Clarendon Press: Oxford, U.K., 1990.
(17) Becke, A. D.; Edgecombe, K. E. *J. Chem. Phys.* **1990**, *92*, 5397.
(18) Bruna, P. J.; Hachey, M. R. J.; Grein, F. *J. Mol. Spectrosc.* **1997**, *400*, 177. Duncan, J. L. *Mol. Phys.* **1974**, *28*, 1177.
(19) Clouthier, D. J.; Ramsay, D. A. *Annu. Rev. Phys. Chem.* **1983**, *34*, 31.
(20) Del Bene, J. E.; Gwaltney, S. R.; Bartlett, R. J. *J. Phys. Chem. A* **1998**, *102*, 5124. Gwaltney, S. R.; Bartlett, R. J. *Chem. Phys. Lett.* **1995**, *241*, 26.
(21) Streitwieser, A.; Kohler, B. *J. Am. Chem. Soc.* **1988**, *110*, 3769.
(22) Fourrē, I.; Silvi, B.; Chaquin, P.; Sevin, A. *J. Comput. Chem.* **1999**, *20*, 897.
(23) Walters, V. A.; Hadad, C. M.; Thiel, Y.; Colson, S. D.; Wiberg, K. B.; Johnson, P. M.; Foresman, J. B. *J. Am. Chem. Soc.* **1991**, *113*, 4782. Wiberg, K. B.; Hadad, C. M.; Foresman, J. B.; Chupks, W. A. *J. Phys.*

Chem. **1992**, *96*, 10756. Hadad, C. M.; Foresman, J. B.; Wiberg, K. B. *J. Phys. Chem*. **1993**, *97*, 4293. Wiberg, K. B.; Hadad, C. M.; Ellison, G. B.; Foresman, J. B. *J. Phys. Chem*. **1993**, *97*, 13586.

(24) Coppens, P. *International Review of Science, Physical Chemistry, Series 2, Vol. 11, Chemical Crystallography*; Robertson, J. M., Ed.; Butterworths: London, 1975; p 21. Dunitz, J. D. *X-ray Analysis and the Structures of Organic Molecules*; Cornell University Press: Ithaca, NY, 1979; Chapter 8.

(25) Wiberg, K. B.; Rablen, P. R. *J. Am. Chem. Soc*. **1995**, *117*, 2201.

(26) Cox, A. P.; Hubbard, S. D.; Kato, H. *J. Mol. Spectrosc*. **1982**, *93*, 196.

(27) Jungen, C.; Merer, A. J. The Renner−Teller Effect. In *Molecular Spectroscopy: Modern Research*; Rao, K. N., Ed.; Academic Press: New York, 1976; p 127.

(28) Kasahara, H.; Mikami, N.; Ito, M.; Iwata, S.; Suzuki, I. *Chem. Phys*. **1984**, *86*, 173.

(29) Tseng, D. C.; Poshutsa, R. D. *J. Chem. Phys*. **1994**, *100*, 7481.

(30) Zhang, Q.; Vaccaro, P. H. *J. Chem. Phys.* **1995**, *99*, 1799.

(31) Brasen, G.; Leidecker, M.; Demtroder, W.; Shimamoto, T.; Kato, H. *J. Chem. Phys*. **1998**, *109*, 2779.

(32) Brown, S. T.; Van Huis, T. J.; Hoffman, B. C.; Schaefer, H. F., III. *Mol. Phys*. **1999**, *96*, 693.

(33) Smith, D. F. J.; Overend, J. *J. Chem. Phys*. **1971**, *54*, 3632.

(34) Buenker, R. J.; Honigmann, M.; Liebermann, H.-P.; Kimura, M. *J. Chem. Phys*. **2000**, *113*, 1046.

(35) Hoy, A. R.; Brand, J. C. D *Mol. Phys*. **1978**, *36*, 1409.

(36) Nachtigall, P.; Hrusak, J.; Bludsky, O.; Iwata, S. *Chem. Phys. Lett*. **1999**, *303*, 441.

(37) Morino, Y.; Tanimoto, M.; Saito, S.; Hirota, E.; Awata, R.; Tanaka, T. *J. Mol. Spectrosc.* **1983**, *98*, 331.

(38) Delon, A.; Jost, R. *J. Chem. Phys*. **1991**, *95*, 5686. Delon, A.; Jost, R.; Jacon, M. *J. Chem. Phys.* **2001**, *114*, 331.

(39) Kukal, V.; Fleurat-Lessard, P.; Schinke, R. *J. Chem. Phys*. **2003**, *119*, 1489. Crawford, T. D.; Stanton, J. F. *J. Chem. Phys.* **2000**, *112*, 7873 (cf. Jackels, C. F.; Davidson, E. R. *J. Chem. Phys*. **1976**, *64*, 2908. Blahous, C. P., III; Yates, B. F.; Schaefer, H. F., III. *J. Chem. Phys*. **1990**, *93*, 8105. Kaldor, U. *Chem. Phys. Lett*. **1991**, *185*, 131).

(40) Aoki, K.; Hoshina, K.-N.; Shibuya, K. *J. Chem. Phys*. **1996**, *105*, 2228 (cf. Shibuya, K.; Terauchi, C.; Sugawara, M.; Aoki, K.; Tsuji, K.; Tsuchiya, S. *J. Mol. Struct.* **1997**, *413*, 501).

(41) Crawford, T. D.; Stanton, J. F.; Szalay, P. G.; Schaefer, H. F., III. *J. Chem. Phys*. **1997**, *107*, 2525.

(42) Frisch, M. J.; Trucks, G. W.; Schlegel, H. B.; Scuseria, G. E.; Robb, M. A.; Cheeseman, J. R.; Montgomery, J. A., Jr.; Vreven, T.; Kundin, K. N.; Burant, J. C.; Millam, J. M.; Iyengar, S. S.; Tomasi, J.; Barone, V.; Mennucci, B.; Cossi, M.; Scalmani, G.; Rega, N.; Petersson, G. A.; Nakatsuji, H.; Hada, M.; Ehara, M.; Toyota, K.; Fukuda, R.; Hasegawa, J.; Ishida, M.; Nakajima, T.; Honda, Y.; Kitao, O.; Nakai, H.; Klene, M.; Li, X.; Knox, J. E.; Hratchian, H. P.; Cross, J. B.; Adamo, C.; Jaramillo, J.; Gomperts, R.; Stratmann, R. E.; Yazyev, O.; Austin, A. J.; Cammi, R.; Pomelli, C.; Ochterski, J. W.; Ayala, P. Y.; Morokuma, K.; Voth, G. A.; Salvador, P.; Dannenberg, J. J.; Zakrzewski, V. G.; Dapprich, S.; Daniels, A. D.; Strain, M. C.; Farkas, O.; Malick, D. K.; Rabuck, A. D.; Raghavachari, K.; Foresman, J. B.; Ortis, J. V.; Cui, Q.; Baboul, A. G.; Clifford, S.; Cioslowski, J.; Stefanov, B. B.; Liu, G.; Liashenko, A.; Piskorz, P.; Komaromi, I.; Martin, R. L.; Fox, D. J.; Keith, T.; Al-Laham, M. A.; Peng, C. Y.; Nanayakkara, A.; Challacombe, M.; Gill, P. M. W.; Johnson, B.; Chen, W.; Wong, M. W.; Gonzalez, C.; Pople, J. A. *Gaussian 03*, revision B.07; Gaussian, Inc.: Pittsburgh, PA 2003.

(43) ACES II is a program product of the Quantum Theory Project, University of Florida, Gainsville, FL. Authors: Stanton, J. F.; Gauss, J.; Perera, S. A.; Yau, A.; Watts, J. D.; Nooijen, M.; Oliphant, N.; Szalay, P. G.; Lauderdale, W. J.; Gwaltney, S. R.; Beck, S.; Balková, A.; Bernholdt, D. E.; Baeck, K.-K.; Rozyczko, P.; Sekino, H.; Huber, C.; Pittner, J. P.; Bartlett, R. J. Integral packages include VMOL (Almlöf, J.; Taylor, P. R.); VPROPS (Taylor, P. R.); ABACUS (Helgaker, T.; Jensen, H. J. Aa.; Jørgensen, P.; Olsen, J.; Taylor, P. R.).

(44) Crawford, T. D.; Sherrill, C. D.; Valeev, E. F.; King, R. A.: psi3@psicode.org

(45) Rablen, P. R. Ph.D. Thesis, Yale University, New Haven, CT, 1994.